Materials Transactions, Vol. 50, No. 12 (2009) pp. 2865 to 2872
©2009 The Japan Institute of Metals

EXPRESS REGULAR ARTICLE

Intragranular Deformation Mechanisms during Ambient-Temperature Creep in Hexagonal Close-Packed Metals

Tetsuya Matsunaga[1,*1], Tatsuya Kameyama[2,*2], Kohei Takahashi[3,*3] and Eiichi Sato[4]

[1]*Department of Space and Astronautical Science, School of Physical Sciences, The Graduate University for Advanced Studies, Sagamihara 229-8510, Japan*
[2]*Department of Materials Engineering, School of Engineering, The University of Tokyo, Tokyo 113-8656, Japan*
[3]*Department of Aerospace Engineering, School of System Design, Tokyo Metropolitan University, Tokyo 191-0065, Japan*
[4]*The Institute of Space and Astronautical Science, Japan Aerospace Exploration Agency, Sagamihara 229-8510, Japan*

Intragranular deformation mechanisms were investigated for ambient-temperature creep of pure hexagonal close-packed (h.c.p.) metals, i.e. commercially pure titanium, pure magnesium and pure zinc, by transmission electron microscopy and electron back-scatter diffraction pattern mapping analysis. First, straightly aligned dislocation arrays were observed in all of the specimens. Second, although the Burgers vectors of $\langle a \rangle$ and several slip systems were observed, only one slip system was activated inside of each grain. Third, the deformation twins that form during creep hinder creep strain. Therefore, the dominant intragranular deformation mechanism of ambient-temperature creep is a planner slip of dislocations inside of a grain. [doi:10.2320/matertrans.M2009224]

(Received June 30, 2009; Accepted September 11, 2009; Published November 11, 2009)

Keywords: *titanium, magnesium, zinc, dislocation structure, ambient-temperature creep*

1. Introduction

The importance of hexagonal close-packed (h.c.p.) metals and alloys, i.e. high-strength titanium (Ti) alloys and magnesium (Mg) alloys, is increasing in the aerospace and transportation industries. However, all h.c.p. metals and alloys show creep behavior at ambient temperature.[1,2] Using Ti-6Al-4V alloy for some critical parts, e.g. bolts and nuts, will bring about stress relaxation, possibly leading a structural component to destruction. Therefore, it is important for the industry to elucidate the mechanism of ambient-temperature creep.

Ambient-temperature creep was observed about one half century ago in pure Ti.[3–5] Since that time, several studies of this phenomenon have been carried out using Ti alloys. Several deformation mechanisms have been proposed based only on those experimental results, which are, in some cases, unique to the tested materials. Several Ti alloys,[6] e.g. Ti-5Al-2.5Sn alloy[7,8] and Ti-6Al-4V alloy,[7,9–11] were investigated in the 1960s and 70s. The main deformation mechanism was interpreted as planar slip of straightly aligned dislocations.[8,10] Later, Mills' group identified the dislocation type for Ti-6Al and Ti-6Al-2Sn-4Zr-2Mo as screw-type with Burgers vectors of $\langle a \rangle$, $\langle c \rangle$ or $\langle c+a \rangle$.[12–17] It was concluded that these straightly aligned dislocations engendered an abnormally low work-hardening exponent and generated ambient-temperature creep.[8,10,13]

Next, Neeraj *et al.*[13] claimed that this creep was identical to Andrade creep.[18,19] Hasija *et al.*[20] used computer simulation to demonstrate the Andrade creep behavior of Ti-6Al alloy. However, the extremely low value of the apparent activation energy that recently reported[21] contradicts that of Andrade creep of 100 kJ/mol.

Third, time-dependent deformation twins were observed in coarse-grained Ti-0.4Mn alloy,[22] with an average grain size of 500 μm, and in Ti-1.6V.[23] Although those results suggest that the deformation twins are yielded in ambient-temperature creep in coarse-grained materials, the role of the deformation twins in a finer-grained sample has not been clear.

As mentioned in the first paragraph, we recently found that all of the h.c.p. metals and alloys show creep behavior at ambient temperature.[24] In our previous paper,[2] the ambient-temperature creep behavior of typical pure h.c.p. metals, i.e. commercially pure Ti (CP-Ti), Mg and zinc (Zn), was summarized: ambient-temperature creep appears below 0.3–0.4 T_m (T_m: melting point) for all h.c.p. metals and alloys. The apparent activation energy in this region is about 20 kJ/mol, the stress exponent is about 3.0 and the grain-size exponent is about 1.0.

The purpose of this study is to reveal the intragranular deformation mechanisms of ambient-temperature creep using several electron microscopy techniques with pure h.c.p. metals, i.e. CP-Ti, Mg and Zn. Transmission electron microscope (TEM) observations, electron back-scatter diffraction pattern mapping (EBSD) analyses and optical microscope (OM) observations were performed for the three pure h.c.p. metals after creep tests at ambient temperature. Using pure metals decreased or negated the effect of solid solution strengthening. Previous works on Ti alloys[8,10,12–17] proposed that solid solute atoms decrease stacking fault energy, generate straightly aligned dislocations, and then brings about ambient-temperature creep in Ti alloys. However, the description of Ti alloys could not explain the creep behavior of pure h.c.p. metals. In addition, using three metals with different crystallographic c/a ratios makes it possible to discuss the differences in the deformation mechanisms through each slip system with the lowest Peierls potential.

*1Graduate Student, The Graduate University for Advanced Studies
*2Graduate Student, The University of Tokyo. Present address: Nagasaki Research Development Center, Mitsubishi Heavy Industries, Ltd., Nagasaki 851-0391, Japan
*3Graduate Student, Tokyo Metropolitan University. Present address: Research and Laboratory Department, Fuji Heavy Industries Ltd. Aerospace Company, Utsunomiya 320-8564, Japan

Table 1 Measured chemical compositions, pre-treatments, crystallographic c/a ratios, and slip systems with the lowest Peierls potential of the four examined specimens.

Samples	Chemical composition* (mass%)	Pre-treatment	c/a	Slip system with the lowest Peiels potential
CP-Ti 1A (grade 1)	Ti-0.03Fe-0.04O-0.002H-0.01C-0.01N	973 K air cooling	1.589	$\langle 11\bar{2}0\rangle\{1\bar{1}00\}$ Prismatic slip
CP-Ti 2 (grade 2)	Ti-0.06Fe-0.09O-0.0002H-0.01C-0.01N	973 K air cooling	1.589	$\langle 11\bar{2}0\rangle\{1\bar{1}00\}$ Prismatic slip
Mg	99.95Mg-0.003Al-0.003Si-.0.008Mn-0.005Zn	573 K hot rolling	1.624	$\langle 11\bar{2}0\rangle\{0001\}$ Basal slip
Zn	99.995Zn	hot rolling	1.856	$\langle 11\bar{2}0\rangle\{0001\}$ Basal slip

*Oxygen contents in CP-Ti sheets were measured by graphite furnace atomic absorption spectrometry.

Finally, we examined the influence of the deformation twin. Creep deformations of Mg in tension and compression were compared because significant deformation twins are well known to decrease compression strength compared to tensile strength. For CP-Ti, the creep behaviors of materials with different oxygen contents were compared because materials with lower oxygen contents generate deformation twins readily.

2. Experimental Procedure

Rolled sheets of CP-Ti (JIS grade 1) designated as CP-Ti 1A, CP-Ti (JIS grade 2) designated as CP-Ti 2, pure Mg and pure Zn with typical rolling textures were used for this work. They are the same sheets as used in our previous paper.[2)] The measured chemical compositions, pre-treatments, c/a ratios, and the lowest Peierls potential slip systems of these sheets are listed in Table 1. The grain sizes, d, were 75, 17, 120 and 100 μm for CP-Ti 1A, CP-Ti 2, Mg and Zn, respectively.

Figure 1 shows the X-ray diffraction (0002) pole figures of CP-Ti 1A, Mg and Zn; the (0002) plane at the specimen's surface (upper) and that in the interior (lower) are shown for each specimen. Although both Mg and Zn show strong rolling textures for the (0002) plane that face the specimen's surfaces ($I_{max} = 45$ and 168, respectively), only pure Mg shows a strong texture, even in the interior of the specimen ($I_{max} = 33$).

TEM observations were performed for CP-Ti 1A, Mg and Zn after creep tests that lasted 4.3×10^5 s under a load of $0.8\sigma_{0.2}$, where $\sigma_{0.2}$ is the 0.2% proof stress. The TEM samples were prepared by twin-jet electro polishing after mechanical grinding to less than 50 μm in thickness with a solution of 6% perchloric acid, 34% 1-butoxyethanol and 60% methanol at a temperature of about 230 K and voltages of 50 V for Mg and 10 V for Zn. For CP-Ti 1A, ion-milling was adopted because hydride particles were readily deposited during electro-polishing. The operating voltage was 300 kV for TEM observation.

The OM observations were executed before and after the creep tests. First, the specimens were polished mechanically using emery papers of up to No. 2400 grit. Then, they were etched using 3 mL of hydrofluoric acid, 6 mL of nitric acid and 100 mL of distilled water for CP-Ti while using 10 mL of nitric acid and 100 mL of distilled water for Mg. Electron back scatter diffraction mapping (EBSD) analysis was performed for CP-Ti 1A and Mg after the creep tests in order to identify the deformation twin type. The specimens were polished mechanically using colloidal silica. They were then etched to remove the adherent oxide film using etchants of 3 mL of hydrofluoric acid, 6 mL of nitric acid and 100 mL of distilled water for CP-Ti while using 10 mL of nitric acid, 20 mL of hydrochloric acid and 70 mL of ethanol for Mg.

3. Experimental Results

3.1 TEM observation: the dislocation structure

To reveal intragranular deformation mechanisms, TEM observations were executed on the specimens of CP-Ti 1A, Mg and Zn that crept at ambient temperature for 4.3×10^5 s under a load of $0.8\sigma_{0.2}$, where $\sigma_{0.2}$ at ambient temperature was 176, 61 and 40 MPa for CP-Ti 1A, Mg and Zn, respectively. The creep curves under these conditions are shown in Fig. 2, where the total true strains are 0.003, 0.021 and 0.048, respectively. Figure 3 depicts the TEM bright field images. The stress axes were perpendicular to the TEM sample's surface. Thus, they were inclined to the micrograph's surface by tilt angles of 1° and 14° for Mg and Zn, respectively. For CP-Ti 1A, the stress axis was parallel to the TEM sample's face because the rolled sheet's thickness was only 1 mm. The beam direction, B, and the g-vector are shown in each figure. These three images show similar dislocation structures: straightly aligned dislocation arrays without any tangled dislocations.

Figure 4 shows an example of the two-plane analysis in Zn, which identifies the dislocation direction, slip plane and dislocation type. The Burgers vector is determined from the two g-vectors that satisfy the invisibility criterion. The dislocation-line direction was determined from the two planes on which the dislocation was located. In this figure, the Burgers vector and dislocation-line direction are determined as $\langle 11\bar{2}0\rangle$ and $\langle 0001\rangle$, respectively; this dislocation belongs to the prismatic slip system with a Burgers vector of $\langle a\rangle$ and a pure edge character. From other observations with different incident axes and g-vectors, no other slip system was observed. Therefore, only one slip system is activated inside this grain.

By analyzing Figs. 3(a)–3(c) in the same way, Burgers vectors of $\langle a\rangle$ are obtained for all three. The obtained slip systems were pyramidal, basal and prismatic. The obtained

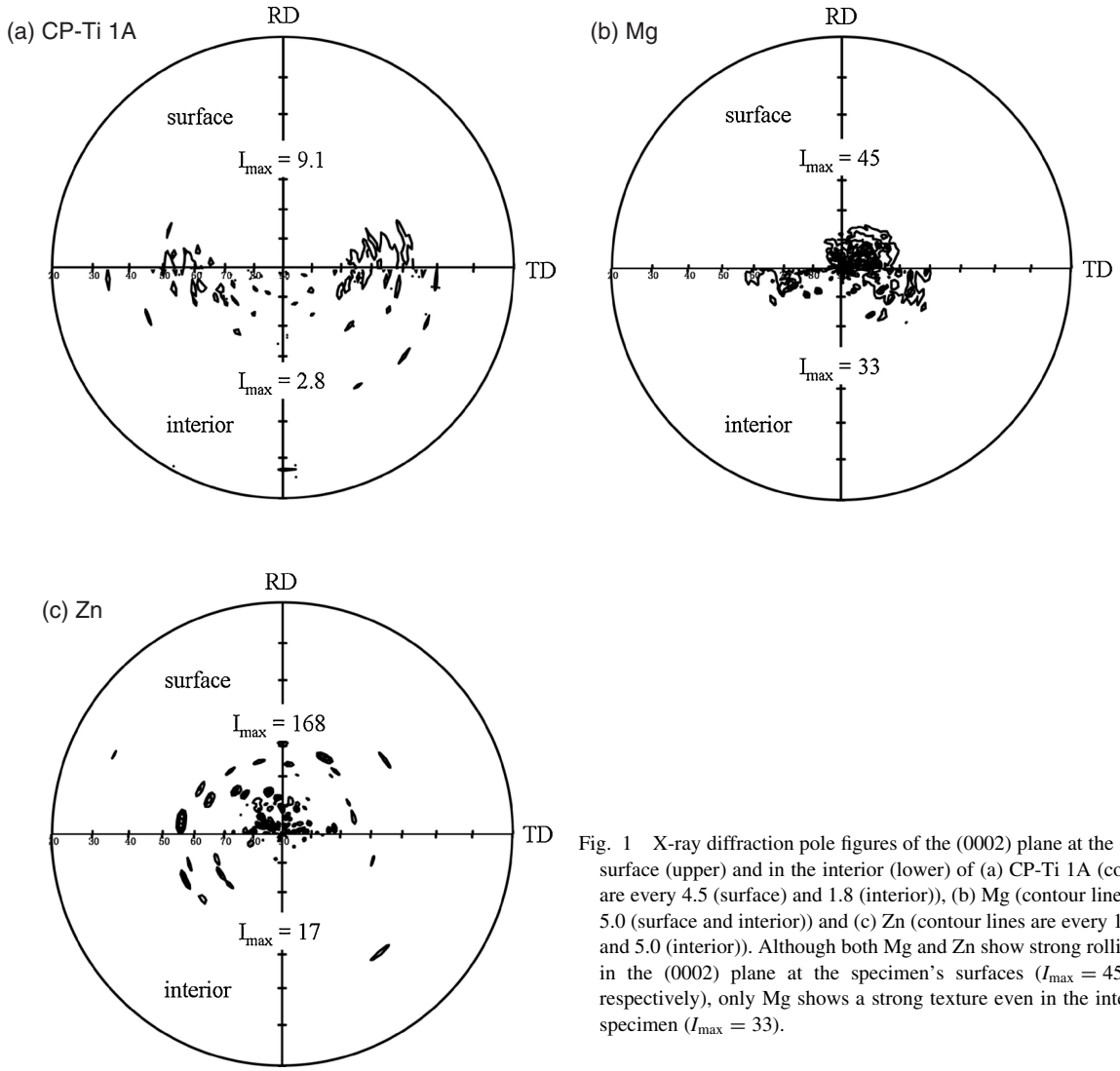

Fig. 1 X-ray diffraction pole figures of the (0002) plane at the specimen's surface (upper) and in the interior (lower) of (a) CP-Ti 1A (contour lines are every 4.5 (surface) and 1.8 (interior)), (b) Mg (contour lines are every 5.0 (surface and interior)) and (c) Zn (contour lines are every 10 (surface) and 5.0 (interior)). Although both Mg and Zn show strong rolling textures in the (0002) plane at the specimen's surfaces ($I_{max} = 45$ and 168, respectively), only Mg shows a strong texture even in the interior of the specimen ($I_{max} = 33$).

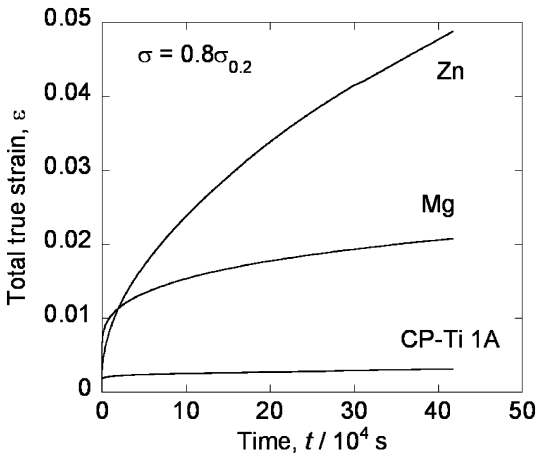

Fig. 2 Creep curves of CP-Ti 1A, Mg and Zn at ambient temperature under the loads of $0.8\sigma_{0.2}$. The total true strains after about 4.3×10^5 s were 0.003, 0.021 and 0.048 for CP-Ti 1A, Mg and Zn, respectively. No materials showed an accelerated creep region.

dislocation types are mixed, mixed and edge dislocation for CP-Ti 1A, Mg and Zn, respectively.

More TEM observations were executed for each metal. In addition to their frequencies of observation, the observed slip systems and dislocation characteristics are listed in Table 2. In CP-Ti 1A, the most frequent slip system and dislocation characteristic were the pyramidal slip $\langle 11\bar{2}0\rangle\{1\bar{1}01\}$ and the mixed dislocation with a dislocation line of $\langle \bar{1}2\bar{1}3\rangle$, respectively. Other slip systems with the basal slip of $\langle 11\bar{2}0\rangle\{0001\}$ and the edge dislocation with a dislocation line of $\langle 0001\rangle$ and the prismatic slip of $\langle 11\bar{2}0\rangle\{1\bar{1}00\}$ and an mixed dislocation with a dislocation line of $\langle \bar{1}2\bar{1}0\rangle$ were also observed. In Mg, the most frequent slip system and dislocation characteristic were the basal slip of $\langle 11\bar{2}0\rangle\{0001\}$ and the mixed dislocation with a dislocation line of $\langle \bar{1}2\bar{1}0\rangle$, respectively. Another slip system with the prismatic slip of $\langle 11\bar{2}0\rangle\{1\bar{1}00\}$ and an edge dislocation with a dislocation line of $\langle 0001\rangle$ was observed. In Zn, the most frequent slip system and dislocation characteristic were the basal slip of $\langle 11\bar{2}0\rangle\{0001\}$ and a screw dislocation with a dislocation line of $\langle 11\bar{2}0\rangle$, respectively. Another slip system with the prismatic slip of $\langle 11\bar{2}0\rangle\{1\bar{1}00\}$ and an edge dislocation with a dislocation line of $\langle 0001\rangle$ was observed.

All of the dislocations in the three metals had Burgers vectors of $\langle 11\bar{2}0\rangle$, but they showed several dislocation-line directions. Consequently, the character was not restricted to that of either an edge or screw type. Although several slip systems were observed, only a single slip system was

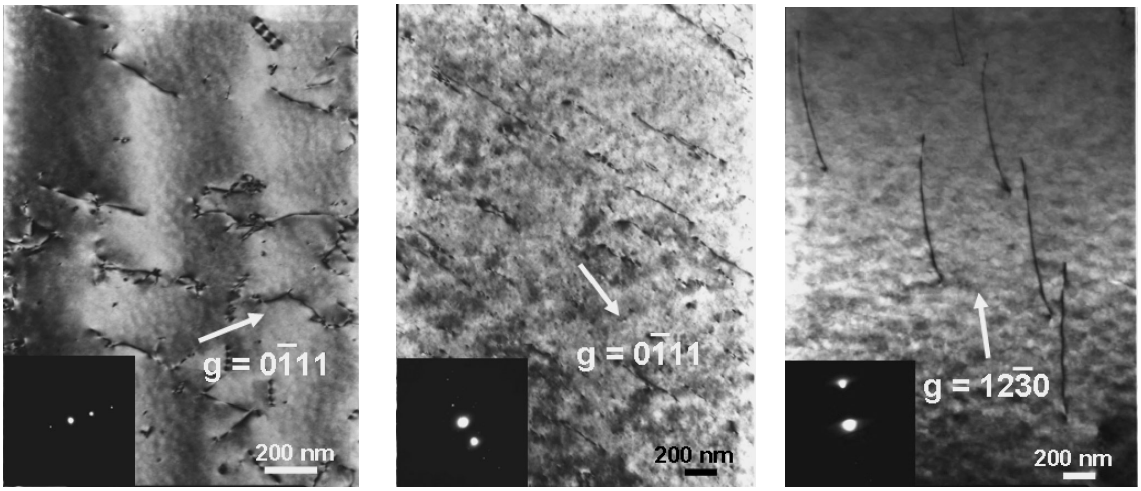

(a) CP-Ti 1A, **B** = [0001] (b) Mg, **B** = [2$\bar{1}\bar{1}$0] (c) Zn, **B** = [0001]

Fig. 3 TEM images were taken after the creep tests: (a) CP-Ti 1A (pyramidal slip with mixed dislocation) at $\varepsilon = 0.003$, (b) Mg (basal slip with mixed dislocation) at $\varepsilon = 0.021$ and (c) Zn (prismatic slip with edge dislocation) at $\varepsilon = 0.048$. All of the images show straightly aligned dislocation arrays without tangled dislocations. The beam direction, B, and the g-vector are shown in each figure.

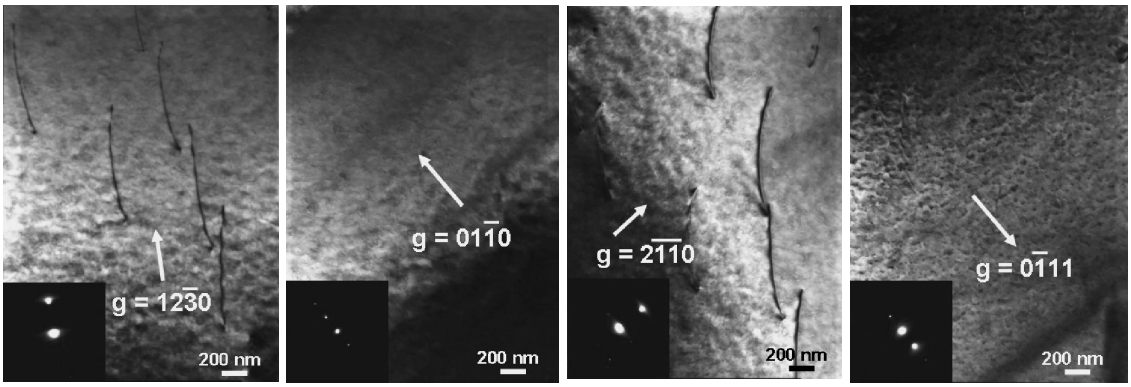

(a) **B** = [0001] (b) **B** = [0001] (c) **B** = [0$\bar{1}$1$\bar{2}$] (d) **B** = [0$\bar{1}$1$\bar{2}$]

Fig. 4 These figures show an example of a two plane analysis of Zn, which identifies the dislocation direction, slip plane and dislocation type. The Burgers vector and dislocation-line direction are determined to be ⟨11$\bar{2}$0⟩ and ⟨0001⟩, respectively; this dislocation belongs to the prismatic slip system with the Burgers vector of ⟨*a*⟩ and a pure edge characteristic.

Table 2 Active slip systems, dislocation characters and observation frequencies for CP-Ti 1A, Mg and Zn crept at ambient temperature for 4.3×10^5 s under loads of $0.8\sigma_{0.2}$, determined using TEM observations.

Samples	Slip system	Dislocation type	*b*	Dislocation direction	Frequency of observation
CP-Ti 1A	⟨11$\bar{2}$0⟩{1$\bar{1}$00} Prismatic slip	Edge dislocation	⟨11$\bar{2}$0⟩	⟨0001⟩	10%
	⟨11$\bar{2}$0⟩{0001} Basal slip	Mixed dislocation	⟨11$\bar{2}$0⟩	⟨$\bar{1}$2$\bar{1}$0⟩	10%
	⟨11$\bar{2}$0⟩{1$\bar{1}$01} Pyramidal slip	Mixed dislocation	⟨11$\bar{2}$0⟩	⟨$\bar{1}$2$\bar{1}$3⟩	80%
Mg	⟨11$\bar{2}$0⟩{0001} Basal slip	Edge dislocation	⟨11$\bar{2}$0⟩	⟨$\bar{1}$2$\bar{1}$0⟩	80%
	⟨11$\bar{2}$0⟩{1$\bar{1}$00} Prismatic slip	Mixed dislocation	⟨11$\bar{2}$0⟩	⟨0001⟩	20%
Zn	⟨11$\bar{2}$0⟩{0001} Basal slip	Screw dislocation	⟨11$\bar{2}$0⟩	⟨11$\bar{2}$0⟩	60%
	⟨11$\bar{2}$0⟩{1$\bar{1}$00} Prismatic slip	Edge dislocation	⟨11$\bar{2}$0⟩	⟨0001⟩	40%

observed inside of each grain. The slip systems were not restricted to that with the lowest Peierls potential; they were strongly influenced by the crystallographic orientation of the grains or the texture. In Mg, for example, although most grains showed a basal slip, which has the lowest Peierls potential, some grains show a prismatic slip because of the strong rolling texture, in which the Schmid factor of the basal slip was almost zero.

3.2 OM observation and EBSD mapping analysis: the influence of deformation twins

Creep tests in tension and compression were executed on pure Mg to reveal the influence of the deformation twins. The applied stresses were identical: 42.7 MPa, which corresponds to $0.7\sigma_{0.2}$ in tension and $1.7\sigma_{0.2}$ in compression. Figure 5 shows the creep curves (a) and their corresponding optical micrographs (b)–(d). The arrows in Fig. 5(a) indicate the

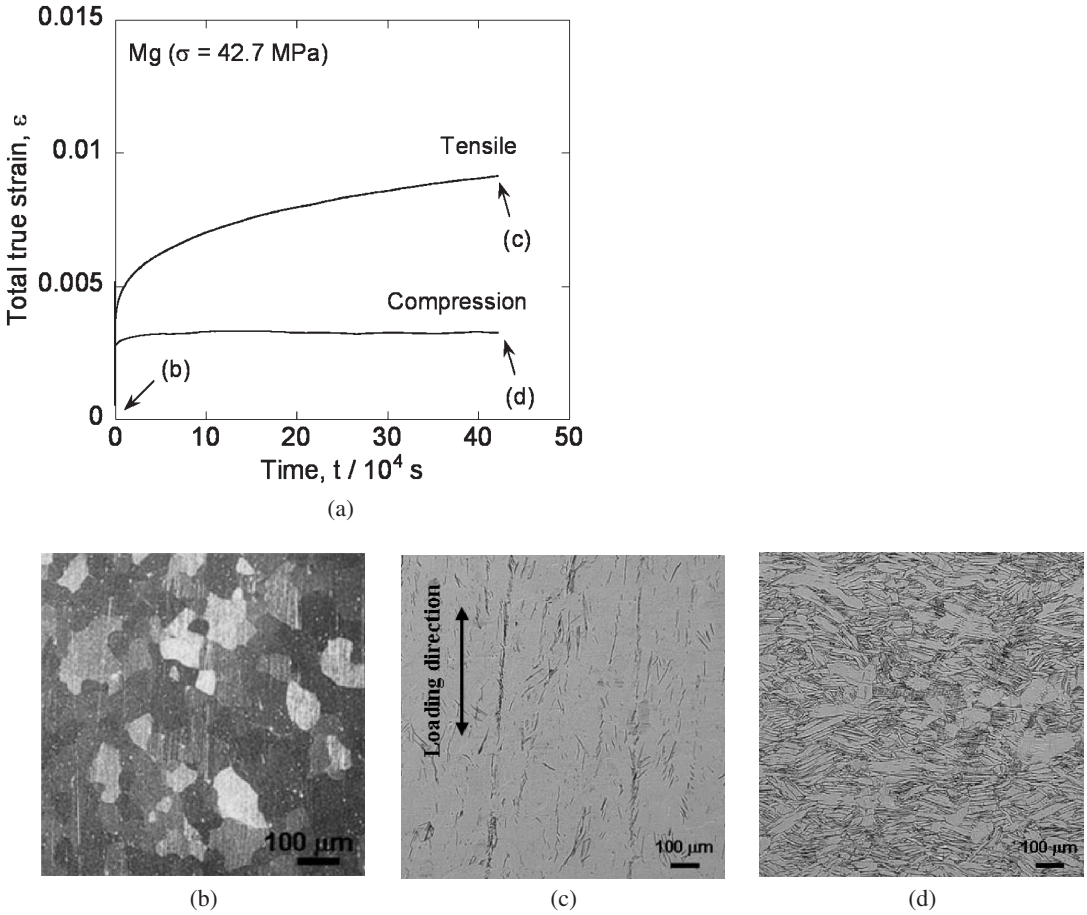

Fig. 5 Comparisons of the creep curves and optical micrographs of Mg between the tensile and compression creep: (a) creep curves, (b) OM image before the test, (c) OM image after the tensile creep test and (d) OM image after the compression creep test under 42.7 MPa for 4.3×10^5 s. Compared to the tensile creep test, innumerable deformation twins have been introduced, and the creep behavior is not significant in the compression creep test. The loading direction is shown in the figure.

Table 3 Misorientation angles along solid lines with the corresponding letters in Fig. 6. All of the misorientations are ca. 86°; the observed deformation twins in Mg are $\langle 10\bar{1}\bar{1}\rangle\{10\bar{1}2\}$ twins.

Range	Misorientation degree	Type of twin
A–B	86°	$\langle 10\bar{1}\bar{1}\rangle\{10\bar{1}2\}$
C–D	87°	$\langle 10\bar{1}\bar{1}\rangle\{10\bar{1}2\}$
E–F	81°	$\langle 10\bar{1}\bar{1}\rangle\{10\bar{1}2\}$
G–H	86°	$\langle 10\bar{1}\bar{1}\rangle\{10\bar{1}2\}$
I–J	85°	$\langle 10\bar{1}\bar{1}\rangle\{10\bar{1}2\}$

observation points of Figs. 5(b)–5(d): before deformation (b) and after creep of 4.3×10^5 s (c), (d). Compared to the tensile creep test, innumerable deformation twins were introduced, while minute creep behavior appeared in the compression creep test.

Deformation twins in compression creep were analyzed using EBSD. The results are represented in Fig. 6; the misorientation angles along several solid lines in Fig. 6 are listed in Table 3. All of the misorientations are around 86°. It is claimed that the most observed deformation twin in Mg is the $\langle 10\bar{1}\bar{1}\rangle\{10\bar{1}2\}$ twin, whose misorientation between twinned and untwined lattices is 86°.[25–27] Another important twin in Mg is the $\langle 10\bar{1}\bar{2}\rangle\{10\bar{1}1\}$ twin, which has a much larger critical resolved shear stress (76–153 MPa) than the

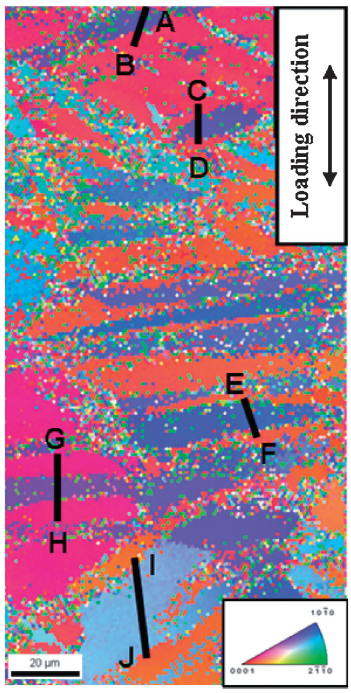

Fig. 6 EBSD map of Mg crept in compression at ambient temperature under $1.7\sigma_{0.2}$ for 4.3×10^5 s. The solid lines with letters in the figure correspond to the analysis points in Table 3.

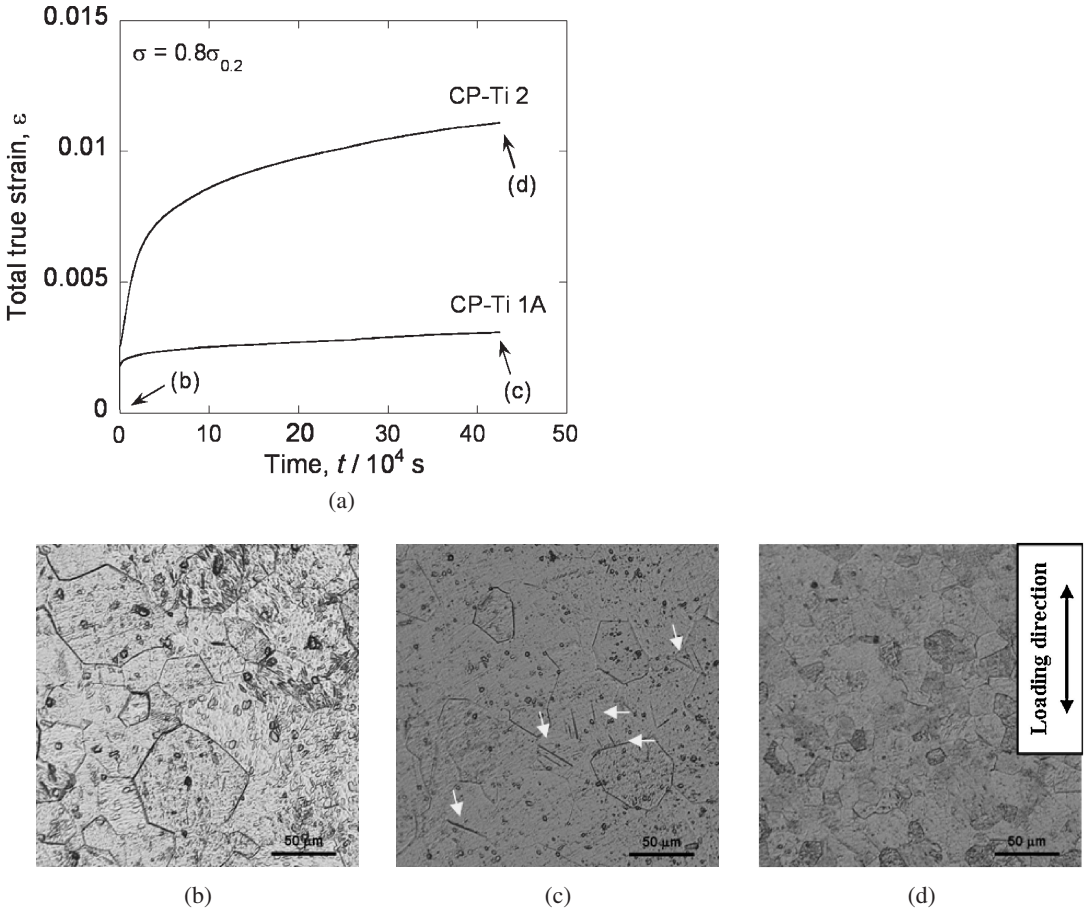

Fig. 7 Comparisons of creep curves and optical micrographs for CP-Ti 1A and 2: (a) creep curves (b) before the creep tests of CP-Ti 1A, (c) after the creep test under $0.8\sigma_{0.2}$ (140 MPa) for 4.3×10^5 s of CP-Ti 1A and (d) after the creep test under $0.8\sigma_{0.2}$ (200 MPa) for 4.3×10^5 s of CP-Ti 2. Larger impurity contents engender more significant creep behavior. These OM images show that the deformation twin, which is indicated by the arrows, exists in the crept CP-Ti 1A sample, although the crept CP-Ti 2 sample shows no deformation twins. The loading direction is shown in the figure.

$\langle 10\bar{1}\bar{1}\rangle\{10\bar{1}2\}$ twin (2 MPa).[25–27] Figure 6 clearly reveals that the deformation twins that forme during a compression creep test at ambient-temperature are $\langle 10\bar{1}\bar{1}\rangle\{10\bar{1}2\}$ twins.

The creep behaviors of CP-Ti 1A ($\sigma_{0.2} = 176$ MPa) and CP-Ti 2 ($\sigma_{0.2} = 280$ MPa) were compared to each other because Ti shows an impurity concentration dependence for generating deformation twins.[28,29] Figure 7 shows creep curves in panel (a) and the corresponding optical micrographs in panels (b)–(d). The applied stresses were 140 MPa and 200 MPa for CP-Ti 1A and CP-Ti 2, respectively, both of which correspond to $0.8\sigma_{0.2}$. The arrows in Fig. 7(a) indicate the points of observation in Figs. 7(b)–7(d): before deformation (a) and after the creep tests of 4.3×10^5 s (c), (d). In fact, CP-Ti 2 shows remarkable creep behavior with a total true strain of 0.012; no deformation twins are observed (Fig. 7(c)), whereas CP-Ti 1A with a low oxygen content shows a reduced creep strain and enhanced deformation twins (Fig. 7(b)). The deformation twins in CP-Ti 1A were analyzed using EBSD as a $\langle 10\bar{1}\bar{1}\rangle\{10\bar{1}2\}$ twin, with very few $\langle 10\bar{1}\bar{2}\rangle\{10\bar{1}1\}$ twins. According to the results and previous works,[28,29] as the impurities in Ti decrease, the deformation twinning becomes significant; then, creep behavior becomes restricted. These experiments on Mg and CP-Ti suggest that activating the deformation twin reduces the ambient-temperature creep.

4. Discussion

A similar intragranular deformation mechanism is operating in all of the tested metals, i.e. straightly aligned dislocation arrays without any tangled dislocations. Although several slip systems are observed in each specimen, it is important that only one slip system (planar slip) is activated inside of each grain. Other slip systems might not be activated in each grain because the h.c.p. structure possesses a low crystalline symmetry. Because few tangled dislocations give a low work-hardening exponent, creep deformation proceeds.

Deformation twins are observed after creep tests of CP-Ti 1A, which contains lower percentage of impurities than CP-Ti 2. In addition, Mg generated more deformation twins during a compression creep test than a tensile creep test. However, their creep strains were much less than that of CP-Ti 2 and the tensile creep test of Mg, respectively. Ankem *et al.*[23] found that the time-dependent deformation twins were the dominant deformation mechanism in Ti-0.4Mn with $d = 500\,\mu$m. Although the deformation twins are introduced during the ambient-temperature creep of coarse-grained Ti, the present results for CP-Ti 1A and Mg reveal that the activation of deformation twins reduce the creep behavior.

Table 4 Comparative table for ambient-temperature creep, high-temperature creep and tensile deformation at ambient temperature. Ambient-temperature creep has peculiar features such as activation of only one slip system, the obviation of the need for accommodation inside of each grain, and the grain-size dependence that results from accommodation at the grain boundary.

	Ambient-temperature creep	High-temperature dislocation creep	Tensile deformation
Inside a grain	Single slip Steady state deformation ↓ Accommodation not necessary	Multiple slip Steady state deformation ↓ Recovery by diffusion	Multiple slip Work hardening ↓ No accommodation
		Is the von Mises' law satisfied?	
At grain boundary	No Grain-size dependence ↓ Accommodation at grain boundary	Yes No grain size dependence	Yes Hall-Petch law

Based on the two findings described above, the intragranular deformation mechanism of ambient-temperature creep in h.c.p. metals is concluded to be straightly aligned dislocation arrays with few tangled dislocations on a single slip system, which gives a low work-hardening exponent.

The von Mises law holds that at least five slip systems must be activated to continue deformation of polycrystalline metals. Therefore, to continue the ambient-temperature creep deformation, an accommodation process must be activated at the grain boundaries. However, abnormally low values of the apparent activation energies of ambient-temperature creep, about 20 kJ/mol,[2] might not activate conventional diffusional accommodation processes. Mordike *et al.*[30] and Koike *et al.*[31] reported exceptionally low apparent activation energies that are close to 20 kJ/mol in several Mg alloys around room temperature. Koike *et al.*[31] also claimed that the deformation is resulted from slip-induced grain boundary sliding (GBS),[32–34] which occurs when the grain boundary dislocations are generated by the dissociating lattice dislocations at the grain boundary, leading to GBS. This mechanism might be activated with extra low apparent activation energy because the diffusion process does not significantly contribute to ambient-temperature creep.

Table 4 is a comparative table that presents information related to ambient-temperature creep, high-temperature dislocation creep and tensile deformation at ambient temperature. It shows intragranular and grain boundary deformation features for each deformation mode. Compared to high-temperature creep and tensile deformation at ambient temperature, ambient-temperature creep has peculiar features: only one slip system is activated, which obviates the need for accommodation inside of each grain, and the grain-size dependence results from accommodation at grain boundaries. The grain boundary functions as a barrier against dislocation motion,[2] unlike conventional dislocation creep at higher temperatures, whose grain-size exponent is nominally zero. This might become a clue to investigate grain boundary phenomena in order to reveal the ambient-temperature creep mechanism, which is now underway.

5. Conclusions

Intragranular deformation mechanisms were investigated by both TEM and OM observations and by EBSD mapping analysis after creep tests at ambient temperature in representative pure h.c.p. metals, i.e., two grades of CP-Ti, pure Mg and pure Zn. This investigation was specifically intended to reveal the activated dislocations and to evaluate the influence of deformation twins. The following conclusions were obtained:

(1) Straightly aligned dislocation arrays with few tangled dislocations were observed in all of the specimens. Creep is considered to proceed at ambient temperature because slow work hardening occurs, which results from weak dislocation interactions.

(2) Although Burgers vectors of $\langle a \rangle$ and several slip systems were observed in the three specimens, only one slip systems was activated inside of each grain. An activated slip system is strongly influenced by the crystallographic orientation or the texture.

(3) Deformation twins of $\langle 10\bar{1}\bar{1} \rangle \{10\bar{1}2\}$ were observed after the creep tests of CP-Ti 1A and Mg in compression. However, their creep behavior was much less significant than that of CP-Ti 2 and Mg in tension, respectively. Consequently, the activation of the deformation twin results in reduced creep behavior.

Acknowledgment

The authors appreciate funding and support, a Grant-in-Aid for Scientific Research from the Japan Society for the Promotion of Science (JSPS) and a JSPS research fellowship for young scientists (00020141), and also those from Integrated Frontier Study, the Light Metal Educational Foundation, Inc.

REFERENCES

1) T. Yamada, K. Kawabata, E. Sato, K. Kuribayashi and I. Jimbo: Mater. Sci. Eng. A **387–389** (2004) 719–722.
2) T. Matsunaga, T. Kameyama, K. Takahashi and E. Sato: Mater. Trans. Submitted.

3) H. Adenstedt: Metal Prog. **56** (1949) 658–660.
4) W. R. Kiessel and M. J. Sinnott: Trans AIME **197** (1953) 331–338.
5) D. R. Luster, W. W. Wentz and D. W. Kaufman: Mater. Methods **37** (1953) 100–103.
6) A. J. Hatch, J. M. Partridge and R. G. Broadwell: J. Mater. **2** (1967) 111–119.
7) T. F. Kiefer and F. R. Schwartzberg: *NASA-CR-92418*, (Martin Co., Denver, CO, USA, 1967).
8) A. W. Thompson and B. C. Odegard: Metall. Trans. A **4** (1973) 899–908.
9) W. H. Reiman: J. Mater. **6** (1971) 926–940.
10) B. C. Odegard and A. W. Thompson: Metall. Trans. A **5** (1974) 1207–1213.
11) M. A. Imam and C. M. Gilmore: Metall. Trans. A **10** (1979) 419–425.
12) S. Suri, G. B. Viswanathan, T. Neeraj, D. H. Hou and M. J. Mills: Acta Mater. **47** (1999) 1019–1034.
13) T. Neeraj, D. H. Hou, G. S. Daehn and M. J. Mills: Acta Mater. **48** (2000) 1225–1238.
14) T. Neeraj and M. J. Mills: Mater. Sci. Eng. A **319–321** (2001) 415–419.
15) M. F. Savage, J. Tatalovich and M. J. Mills: Phil. Mag. **84** (2004) 1127–1154.
16) T. Neeraj, M. F. Savage, J. Tatalovich, L. Kovaric, R. W. Hayes and M. J. Mills: Phil. Mag. **85** (2005) 279–295.
17) D. Deka, D. S. Joseph, S. Ghosh and M. J. Mills: Metall. Mater. Trans. **37A** (2006) 1371–1388.
18) A. W. Cottrell: Philos. Mag. **74** (1996) 1041–1046.
19) A. W. Cottrell: Philos. Mag. Lett. **75** (1997) 301–307.
20) V. Hasija, S. Ghosh, M. J. Mills and D. S. Joseph: Acta Mater. **51** (2003) 4533–4549.
21) H. Tanaka, T. Yamada, E. Sato and I. Jimbo: Scr. Mater. **54** (2006) 121–124.
22) S. Ankem, C. A. Greene and S. Singh: Scr. Metall. **30** (1994) 803–808.
23) A. K. Aiyanger, B. W. Neuberger, P. G. Orberson and S. Ankem: Metall. Mater. Trans. **36A** (2005) 637–644.
24) E. Sato, T. Yamada, H. Tanaka and I. Jimbo: Mater. Trans. **47** (2006) 1121–1126.
25) H. Yoshinaga and R. Horiuchi: Trans. JIM **4** (1963) 1–8.
26) B. C. Wonsiewicz and W. A. Backofen: Trans. Metall. Soc. AIME **239** (1967) 1422–1431.
27) R. E. Reed-Hill and W. D. Robertson: Acta Metall. **5** (1957) 717–727.
28) S. Nemat-Nasser, W. G. Guo and J. Y. Cheng: Acta Mater. **47** (1999) 3705–3720.
29) D. H. Shin, I. Kim, J. Kim and Y. T. Zhu: Mater. Sci. Eng. A **334** (2002) 239–245.
30) B. L. Mordike: Mater. Sci. Eng. A **324** (2002) 103–112.
31) J. Koike, R. Ohyama, T. Kobayashi, M. Suzuki and K. Maruyama: Mater. Trans. **44** (2003) 445–451.
32) Y. Ishida and M. H. Brown: Acta Metall. **15** (1967) 857–860.
33) R. Z. Valiev and O. A. Kaibyshev: Phys. Status Solidi (a) **44** (1977) 477–484.
34) P. Mussot, C. Rey and A. Zaoui: Res. Mech. **14** (1985) 69–79.